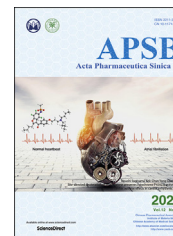




Chinese Pharmaceutical Association
Institute of Materia Medica, Chinese Academy of Medical Sciences

Acta Pharmaceutica Sinica B

www.elsevier.com/locate/apsb
www.sciencedirect.com



ORIGINAL ARTICLE

Cucurbitacin B-induced G2/M cell cycle arrest of conjunctival melanoma cells mediated by GRP78–FOXM1–KIF20A pathway



Jinlian Wei^{a,†}, Xin Chen^{a,†}, Yongyun Li^{b,†}, Ruoxi Li^a, Keting Bao^a,
Liang Liao^a, Yuqing Xie^a, Tiannuo Yang^a, Jin Zhu^a, Fei Mao^a,
Shuaishuai Ni^c, Renbing Jia^b, Xiaofang Xu^{b,*}, Jian Li^{a,d,e,f,*}

^aState Key Laboratory of Bioreactor Engineering, Shanghai Frontiers Science Center of Optogenetic Techniques for Cell Metabolism, Frontiers Science Center for Materiobiology and Dynamic Chemistry, Shanghai Key Laboratory of New Drug Design, School of Pharmacy, East China University of Science and Technology, Shanghai 200237, China

^bDepartment of Ophthalmology, Ninth People's Hospital, Shanghai Jiao Tong University School of Medicine, Shanghai 200025, China

^cCancer Institute, Longhua Hospital, Shanghai University of Traditional Chinese Medicine, Shanghai 200032, China

^dYunnan Key Laboratory of Screening and Research on Anti-pathogenic Plant Resources from West Yunnan, College of Pharmacy, Dali University, Dali 671000, China

^eClinical Medicine Scientific and Technical Innovation Center, Shanghai Tenth People's Hospital, Tongji University School of Medicine, Shanghai 200092, China

^fKey Laboratory of Tropical Biological Resources of Ministry of Education, College of Pharmacy, Hainan University, Haikou 570228, China

Received 7 January 2022; received in revised form 2 April 2022; accepted 7 April 2022

KEY WORDS

Conjunctival melanoma;
Cucurbitacin B;
Activity-based protein
profiling;

Abstract Conjunctival melanoma (CM) is a rare and fatal malignant eye tumor. In this study, we deciphered a novel anti-CM mechanism of a natural tetracyclic compound named as cucurbitacin B (CuB). We found that CuB remarkably inhibited the proliferation of CM cells including CM-AS16, CRMM1, CRMM2 and CM2005.1, without toxicity to normal cells. CuB can also induce CM cells G2/M cell cycle arrest. RNA-seq screening identified KIF20A, a key downstream effector of FOXM1

*Corresponding authors.

E-mail addresses: jianli@ecust.edu.cn (Jian Li), xuxu0139@hotmail.com (Xiaofang Xu).

[†]These authors make equal contributions to this work.

Peer review under responsibility of Chinese Pharmaceutical Association and Institute of Materia Medica, Chinese Academy of Medical Sciences.

<https://doi.org/10.1016/j.apsb.2022.05.021>

2211-3835 © 2022 Chinese Pharmaceutical Association and Institute of Materia Medica, Chinese Academy of Medical Sciences. Production and hosting by Elsevier B.V. This is an open access article under the CC BY-NC-ND license (<http://creativecommons.org/licenses/by-nc-nd/4.0/>).

G2/M cell cycle;
GRP78;
FOXM1;
KIF20A;
Rare tumor

pathway, was abolished by CuB treatment. Further target identification by activity-based protein profiling chemoproteomic approach revealed that GRP78 is a potential target of CuB. Several lines of evidence demonstrated that CuB interacted with GRP78 and bound with a K_d value of 0.11 $\mu\text{mol/L}$. Furthermore, ATPase activity evaluation showed that CuB suppressed GRP78 both in human recombinant GRP78 protein and cellular lysates. Knockdown of the *GRP78* gene significantly induced the downregulation of FOXM1 and related pathway proteins including KIF20A, underlying an interesting therapeutic perspective. Finally, CuB significantly inhibited tumor progression in NCG mice without causing obvious side effects *in vivo*. Taken together, our current work proved that GRP78–FOXM1–KIF20A as a promising pathway for CM therapy, and the traditional medicine CuB as a candidate drug to hinder this pathway.

© 2022 Chinese Pharmaceutical Association and Institute of Materia Medica, Chinese Academy of Medical Sciences. Production and hosting by Elsevier B.V. This is an open access article under the CC BY-NC-ND license

(<http://creativecommons.org/licenses/by-nc-nd/4.0/>).

1. Introduction

Conjunctival melanoma (CM) is a rare and life-threatening malignancy of the melanocytes, located in the ocular surface. It accounts for about 2% of all the ocular tumors and 1.6% of all the non-cutaneous melanomas^{1,2}. The reported incidences of CM are 0.2–0.5 per million in Caucasian populations and 0.15 per million in Asian population^{3,4}. Mostly CM arises from the primary acquired melanosis (PAM) or conjunctival pigmented nevus⁵. It could originate from any part of the conjunctiva and quickly invade other structures of the eye. The uncontrolled disease metastases typically occur in ears, nose, neck, lung, liver, skin and even brain^{3,6}. The available statistics indicates that CM shows a ten-year local recurrence rate in 50% of the cases and distant metastases are diagnosed in 26% of the cases⁶. To date, there is no more extensive elucidation about genetic and epigenetic characteristics of CM. As reported, CM shares many typical genetic alterations with both cutaneous melanoma and other mucosal melanomas⁶. Ras–Raf–MEK–ERK (mitogen-activated protein kinase [MAPK]) and phosphatidylinositol-3-kinase (PI3K)–AKT–mammalian target of rapamycin (mTOR) pathways are frequently overactivated in CM cells^{7,8}. *BRAF* and *NRAS* mutations are commonly found in CM, with incidences of 14%–50% and 18%, respectively^{9–14}. Besides, abnormal expression of cellular proteins including PTEN, Hsp90, Bcl-2, P16INK4a, EZH2 and TERT are also detected in CM cells¹⁵.

Current treatment for the CM includes wide local excision, combined with adjunct treatment with chemotherapy such as mitomycin C (MMC) and interferon alpha-2b (IFN- α 2b), radiotherapy and cryotherapy⁶. However, the side-effects caused by the typical chemotherapy are severe and there is no more other effective treatment strategy for it. Given the genetic similarity between CM and cutaneous melanoma, prospective potential treatments for CM includes investigating new targeted therapies, the strategy which has been found to be effective for cutaneous melanoma¹⁶. It could be understood by the clinical cases treated with marketed *BRAF* inhibitors alone or in combination with MEK inhibitors which have shown favorable effect on relieving the symptoms of the CM^{14,17–19}. Till date, no drugs targeting *BRAF* or *NRAS* mutations in CM have been approved by the US Food and Drug Administration (FDA). What makes CM more difficult to cure are its rare incidences among the population, extremely complex pathogenesis, and long incubation period⁶. Scanning the drug development process thoroughly, it has been

found that the orphan drugs for the rare diseases have long been neglected owing to the considerable costs and challenges²⁰. In such scenario, repurposing of the clinically approved drugs and compounds would provide an alternative approach for drug development especially for rare diseases. Our group has long focused on drug repurposing and accelerated drug development and mechanism study in certain diseases, such as cancer²¹, malaria^{22,23}, Methicillin-resistant *Staphylococcus aureus* infection²⁴, Alzheimer's disease²⁵ and aging²⁶. In our previous research, we conducted a cell-based drug repurposing phenotypic screening, and disclosed FUBP2 as a druggable target of fanchinoline against CM²⁷. However, the understanding of the CM pathogenesis and novel therapeutic targets for the CM therapy is far from completeness.

In the present study, we attempted to reveal more potential drugs and targets that could be adopted in therapy of CM. Fortunately, we discovered, for the first time to the best of our knowledge, cucurbitacin B (CuB) exhibited potent anti-proliferative activity against CM cells with typical *NRAS* and *BRAF* mutations including CRMM2, CM-AS16, CRMM1 and CM2005.1 (Table 1). CuB is one of the most abundant and commonly investigated cucurbitacins derivatives, which are tetracyclic compounds isolated from Cucurbitaceae plants. It is a traditional medicine, with multiple pharmacologic activities such as anti-inflammatory, antipyretic, anti-diabetic and anticancer activities which are mediated by different regulating signaling pathways^{28–30}. In China, CuB has been used as an adjuvant treatment agent for chronic hepatitis and primary liver cancer. Although different anticancer mechanisms of CuB have been investigated, most of them are downstream pathways and relative effectors^{31–36}.

Table 1 *In vitro* antiproliferative activity of CuB against CM and normal cells.

Cell line	Anti-proliferation IC ₅₀ ($\mu\text{mol/L}$)	
	CuB	MEK162
CRMM2	0.15 \pm 0.01	0.0226 \pm 0.0004
CM-AS16	0.08 \pm 0.01	0.0085 \pm 0.0003
CRMM1	0.24 \pm 0.01	0.0061 \pm 0.0002
CM2005.1	0.38 \pm 0.02	0.0071 \pm 0.0002
HL7702	>100	>100

Data are shown as mean \pm SD, $n = 3$. MEK162 as the positive control.

Our current work demonstrated that CuB could lead to the arrest of the cell cycle and FOXM1–KIF20A pathway in CM cells which was confirmed by the transcriptome analysis. Further activity-based protein profiling (ABPP) chemoproteomic approach revealed that one of the primary targets of CuB in CM cells is GRP78 protein. Inhibition of GRP78 by CuB or *GRP78* knockdown aggravated the suppression of the GRP78 ATPase enzymatic activity and its downstream proteins expression such as KIF20A, Cyclin B1 and CDK1 through FOXM1 pathway. More importantly, GRP78–FOXM1–KIF20A pathway was also inhibited after CuB treatment in the *in vivo* anti-tumor evaluation. Our research indicated GRP78–FOXM1–KIF20A as an important pathway in CM progression, and CuB as a potential traditional medicine to intervene this pathway in such rare ocular tumor treatment.

2. Materials and methods

2.1. Reagents

Cucurbitacin B (98%) was purchased from the Nanjing Sen-BeiJia Biological Technology Co., Ltd. (SBJ-I0498, Jiangsu, China). MEK162 was purchased from the CSNpharm (CSN16001, Chicago, USA). Fetal bovine serum (FBS, 42F6590K), RPMI-1640 medium HEPES (1640H, 22400089) and Ham's F12K (Kaighn's) medium (F12K, 21127022) were from Gibco (NY, USA). Phosphate buffer solution (PBS), phenylmethanesulfonyl fluoride (PMSF, 20104ES03), RIPA lysis buffer (20114ES60), penicillin–streptomycin (60162ES76), Super ECL Detection Reagent (36208ES60) were from Yeasen (Shanghai, China). Serum-free cell freezing medium was from NCM Biotech Co., Ltd. (C40050, Suzhou, China). Cell counting kit-8 (CCK-8) was procured from TargetMol (C0005, Boston, USA). Cell Cycle and Apoptosis Analysis Kit (C1052), Annexin V-FITC Apoptosis Detection Kit (C1062M) and Fast Silver Stain Kit (P0017S) were procured from Beyotime Biotechnology (Jiangsu, China). Multicolor protein markers were from Biorad (161-0394, CA, USA) and Yeasen (20352ES76, Shanghai, China). Polyvinylidene fluoride (PVDF) was from Merck Millipore (IPVH00010, Darmstadt, Germany).

2.2. Cell source and culture

Conjunctival melanoma cell lines CRMM1, CRMM2 and CM2005.1 were generously provided by Prof. Martine J. Jager (Leiden University Medical Center, Leiden, The Netherlands)¹⁶, CMAS16 was provided by Professor Renbin Jia (Shanghai Ninth People's Hospital, Shanghai, China)³⁷. Human embryonic kidney HEK293T (CRL-3216) was obtained from American Type Culture Collection. CM-AS16 and CM2005.1 were maintained in 1640H medium, CRMM1 and CRMM2 were maintained in F12K medium. HEK293T cells were maintained in DMEM medium. All of the mediums were supplemented with 10% FBS, streptomycin (100 µg/mL), and penicillin (100 U/mL). Cells were then cultured in these mediums at 37 °C in an incubator with humidified atmosphere of 5% CO₂.

2.3. Cell proliferation assay

100 µL cells were seeded in triplicate in 96-well culture plates at a confluency of 70%–80% per well (about 1×10^4 cells/well). Next day, cells were treated with 100 µL of fresh medium with different concentrations of the test compounds and incubated for

72 h. After removing the medium, the cells were administered with 100 µL medium containing 10% CCK-8 reagent and re-incubated for 1 h. Then, the absorbance at 450 nm was measured in a microplate reader (Synergy H1, Biotek, Vermont, USA). The readings were normalized to the DMSO-treated cells, and inhibitory concentration (IC₅₀) values were calculated by GraphPad Prism 8.0.

2.4. Cell cycle assay

Cells were grown to the 80%–90% confluency in 6-well plates and synchronized by culturing in serum-free F12K medium for 12 h, following by 24 h treatment of different concentrations of CuB. Subsequently, cells were trypsinized and fixed in ice-cold 70% ethanol for overnight at –20 °C. Cells were then centrifugated and the pellet was resuspended in PBS, stained using cell cycle staining solution according to the protocol provided by the Cell Cycle and Apoptosis Analysis Kit. Cell cycle analysis was performed using a flow cytometer (CytoFLEX LX, Beckman Coulter, CA, USA). The analysis of the obtained data was carried out using FlowJo software. The results were analyzed using statistical methods.

2.5. Apoptosis analysis

Cells were grown to the 80%–90% confluency in 6-well plates as described above. Cell apoptosis was determined by flow cytometry using the Annexin V-FITC Apoptosis Detection Kit according to the manufacturer's instructions. Cultured cells were harvested after 24 h CuB treatment, incubated with 5 µL of Annexin V-FITC and then incubated with 10 µL of PI for 20 min at room temperature, resuspension buffer. These stained cells were then analyzed using a flow cytometer and FlowJo software.

2.6. Transcriptome analysis by RNA-seq

1×10^8 CRMM2 cells were cultured in 10 cm dishes and treated with DMSO/0.1 µmol/L CuB/0.2 µmol/L CuB. The transcriptome analysis by RNA-seq was performed according to a previously published method³⁸. Total RNA was extracted from cell samples using TRIzol Reagent (R0016, Beyotime, Shanghai, China). RNA-seq transcriptome library was prepared following Tru-Seq™ RNA sample preparation Kit from Illumina (CA, USA) using 1 µg of total RNA. Illumina HiSeq Xten/NovaSeq 6000 systems was used for sequencing. Fragments per kilobase of exon model per million mapped reads (FKPM) of every mRNA were used for the further analysis. More detailed protocols were assisted by Majorbio Bio-Pharm Technology Co., Ltd. (Shanghai, China). The accession number for RNA-seq reported in this paper is GEO:GSE 192359.

2.7. qRT-PCR analysis

Cells were grown to 80%–90% confluency in 6-well plates as described above. Different concentrations of CuB in fresh medium (the total volume was 1.5 mL, DMSO < 0.01%) were added to the wells and incubated for 24 h. Total RNA was extracted from CRMM2 cells using a Total RNA Kit II (R6934-01, Omega, USA) and reverse transcribed with Hifair II 1st Strand cDNA Synthesis SuperMix for qPCR (11123ES60, Yeasen, Shanghai, China) according to the manufacturer's instructions. QPCR was performed

using Hieff qPCR SYBR® Green Master Mix (11201ES08, Yeasen, Shanghai, China) on a quantitative PCR system (CFX96 Touch, Bio-Rad, CA, USA). *GAPDH* was used as an internal control. Primers used for performing qPCR have been listed as follows: for *GAPDH*, Forward 5'-AAGGTGAAGGTCCGAGTCAAC-3', Reverse 5'-GGGGTCATTGATGGCAACAATA-3'; for *KIF20A*, Forward 5'-CAAGAGGCAGACTTTGCGGCTA-3', Reverse 5'-GCTCTGGTCTTACGACCCACT-3'; for *FOXM1*, Forward 5'-TCTGCCAATGGCAAGGTCTCCT-3', Reverse 5'-CTGGATTCGGTCGTTTCTGCTG-3'; for *PLK1*, Forward 5'-GCACAGTGTCAATGCCTCCAAG-3', Reverse 5'-GCCGTACTTGTCGAATAGTCC-3'.

2.8. Western blot analysis

Western blot analysis was performed as described previously²⁷. Cells were grown to 80%–90% confluency in 6-well plates as described above and lysed in RIPA lysis buffer supplemented with 1 mmol/L PMSE. The proteins were separated by SDS-PAGE, transferred onto PVDF membranes and then incubated with the appropriate primary antibodies. Primary antibodies against Cyclin B1 (ab181593, Abcam), CDK1 (ab1333327, Abcam), KIF20A (ab70791, Abcam), PLK1 (ab189139, Abcam), FOXM1 (ab207298, Abcam), GRP78 (3177T, Cell Signaling), Bax (AF1270, Beyotime), caspase-3 (AF0081, Beyotime), cleaved-PARP1 (ab32064, Abcam), Bcl-2 (ab32124, Abcam), p21 (sc-6246, Santa Cruz), p53 (sc-126, Santa Cruz), HSP90 (ab282108, Abcam), GAPDH (60004-1-Ig, Proteintech) and Vinculin (ab129002, Abcam) were used. Secondary antibodies HRP-linked anti-rabbit IgG antibody (7074S, Cell Signaling) and HRP-linked anti-mouse IgG antibody (7076S, Cell Signaling) were further used. Finally, proteins were visualized with the ECL System from Tanon (4600SF, China).

2.9. In-gel fluorescence analysis

In-gel fluorescence analysis were performed as previously described³⁹. Cells were grown to 80%–90% confluency in 6-well plates as described above and treated with 0.2 μmol/L probes for 3 h. The cells were then washed with 1 × PBS, rapidly trypsinization and centrifugated to the collect cell pellets, which were sonicated to obtain the total cell proteome solution. A freshly prepared click chemistry reaction cocktail containing 20 μmol/L TAMRA-N₃, 50 μmol/L TBTA, 0.5 mmol/L TCEP and 0.5 mmol/L CuSO₄ was added to the cell proteome and further incubated for 2 h at room temperature. The reaction was quenched by addition of pre-chilled acetone to the precipitated proteins. The resulted proteins were subsequently collected by centrifugation (12,000 × g, 15 min at 4 °C), and washed with pre-chilled methanol. The samples were dissolved in 1 × SDS loading buffer and thermal denaturation was done at 95 °C for 10 min. 20 μg proteins for each lane were loaded on SDS-PAGE (10% gel) and then visualized by in-gel fluorescence scanning (Typhoon Trio, GE).

For recombinant protein labeling, different concentration gradients of probes were incubated with purified GRP78 protein at different final concentrations in PBS buffer for 1 h at 37 °C with gentle shaking. The subsequent labeling processes were similar to that of cell total proteome mentioned above. Purified GRP78 protein was purchased from Abcam (ab78432), purified mutant GRP78 (Lys326Ala) was obtained at the aid of Zoonbio Biotechnology Co., Ltd. (Nanjing, China).

2.10. Cellular imaging

Fluorescence microscopy was performed to demonstrate the ability of the probes for cellular targets imaging. CRMM2 cells seeded in the glass bottom dishes were grown to 70%–80% confluency, incubated with probes F12K solution. After treatment for 3 h, cells were washed with PBS gently. Following procedures included 1 h of cell immobilization with 3.7% formaldehyde, 1 h of permeabilization with 0.1% Triton X-100, and 2 h of click chemistry reaction in the freshly premixed click chemistry reaction cocktail. Then, cells were washed with PBS twice and 0.1% Tween 20 in PBS for once. At last, the cells were stained with DAPI (G1012, Servicebio, 1:1000 dilution in PBS) for 5 min at room temperature prior to imaging. For co-localization experiments, cells were further incubated with anti-GRP78 antibody (1:100) for overnight at 4 °C, washed twice with PBS, and then incubated with Alexa Fluor 488 goat anti-rabbit IgG(H+L) (ab150077, Abcam, 1:1000 dilution in PBS) for 1 h, following by washing again. Confocal fluorescence images were measured by a Leica confocal microscope (TCS SP8, Leica, Germany).

2.11. Pull down/LC-MS/MS

To identify the potential interacting cellular targets of **BP-2**, pull-down experiments were carried out, accompanied by Western blot (WB) and LC-MS/MS analysis. CRMM2 cells were grown in 10 cm dishes to 90% confluency and treated with probe-containing medium (FBS free) in the presence or absence of corresponding competitors. After 3 h of incubation, cells were harvested and lysed by sonication (4 × 2 s on, 3 s off, 20% amplitude). The total protein concentration was determined by BCA Protein Quantification Kit (20201ES76, Yeason) and was diluted to final concentration of 1 mg/mL. A freshly premixed click chemistry reaction cocktail was added (20 μmol/L Biotin-N₃, 50 μmol/L TBTA, 0.5 mmol/L TCEP, and 0.5 mmol/L CuSO₄). The reaction was incubated for 2 h with gentle mixing and further precipitated by the addition of the pre-chilled acetone (−20 °C). The resulted proteins were subjected to centrifugation (12,000 × g, 15 min at 4 °C) to remove the redundant click reagents. The obtained supernatants were incubated with Capturem Streptavidin Miniprep Columns (635733, Takara) at room temperature for 30 min. The columns were washed three times with PBS to remove unbound proteins, the streptavidin-bound proteins were eluted with a buffer containing 0.1 mol/L glycine (pH 2.5), neutralized in a buffer containing 1 mol/L Tris (pH 8.5), separated by SDS-PAGE, and visualized by silver staining. Enriched protein bands were excised and washed until opaque and stick using 30 mmol/L K₃Fe(CN)₆ and 100 mmol/L Na₂S₂O₃ (1:1). For alkylation, 50 mmol/L IAA in 50 mmol/L NH₄HCO₃ buffer was added to completely cover the gel slices and incubated for 60 min at room temperature in the dark. Supernatant was then removed and washed with ACN solution. For the digestion, 5–20 μL of enzyme digestion solution was added to keep the gel pieces wet during the enzymatic digestion. The reaction was incubated overnight at 37 °C. Extraction solution (5% TFA–50% ACN–45% ddH₂O) was added to the gel pieces to quench the digestion reaction. The resulting peptides supernatant was transferred to a new tube, desalted with Waters C18 Tips and lyophilized by vacuum centrifugation. Peptides were resuspended in 10 μL of 0.1% formic acid before the LC-MS/MS analysis. The peptides were separated and analyzed on an Ultimate 3000 system coupled to a

Q Exactive™ Hybrid Quadrupole-Orbitrap™ Mass Spectrometer (both Thermo Scientific). About 5 μ L of peptides were separated to an in-house made column (150 μ m \times 15 cm) packed with C18 AQ (1.9 μ m, 100 \AA , Dr. Maisch GmbH, Germany) at a flow rate of 600 nL/min. Mobile phase A (0.1% formic acid in 2% ACN) and mobile phase B (0.1% formic acid in 98% ACN) were used to establish a 66 min gradient comprised of 2 min of 4%–8% B, 43 min of 8%–28% B, 10 min of 28%–40% B, 1 min of 40%–95% B, and 10 min of 95% B. Peptides were then ionized by electrospray at 2.2 kV. A full MS spectrum (m/z range 300–1800) was acquired at a resolution of 70,000 at m/z 400 and a maximum ion accumulation time of 40 ms. The raw data were processed and searched with MaxQuant 1.6.2.10 with MS tolerance of 20 ppm, and MS/MS tolerance of 20 ppm. All the LC–MS/MS analysis were provided by Bio-Tech Pack Technology Company Ltd. (Beijing, China).

2.12. GRP78 ATPase enzymatic activity

GRP78 ATPase enzymatic activity was measured using a malachite green-phosphate assay (10009325, Cayman) as described in previous report⁴⁰. All samples were diluted in an assay buffer consisting of 20 mmol/L Tris (pH 7.5), 50 mmol/L KCl, and 1.5 mmol/L MgCl₂. Assays to determine inhibition of ATPase activity were done with GRP78 (0.25 μ mol/L), with CuB (0–100 μ mol/L). 20 μ L working reagent (10009325, Cayman) was added to an 80 μ L tested samples containing different concentrations of CuB and recombinant human GRP78 protein (ab78432; Abcam). The mixtures were then incubated for 30 min at room temperature for color development and absorbance was measured at 620 nm on a plate reader (Synergy H1, Biotek, Vermont, USA).

2.13. MST (microscale thermophoresis) assay

To evaluate the binding affinity of CuB and GRP78, an MST assay was conducted by Monolith NT. Automated (NanoTemper Technologies). Recombinant his-tag GRP78 protein was labelled with RED-tris-NTA 2nd generation dye solution (MO-L018, NanoTemper Technologies) according to the manufacturer's instructions. The final labelled GRP78 protein concentration was 50 nmol/L, which was mixed with different concentrations of CuB by pipetting up and down multiple times. All samples were diluted in 1 \times PBST and contained the same amount of DMSO. The K_d was determined in MO. Control using the K_d fit.

2.14. Cell transfection

Taitool Bioscience (Shanghai, China) assisted the construction of recombinant adenovirus vector systems of GRP78 knockdown and over-expression. CM cells were seeded into six-well culture plates with 1 \times 10⁵ cells per well in corresponding culture medium plus 10% FBS. After adherence, cells were transfected by adding the adenovirus particles to the culture at an MOI of 100 for 24 h. For Western blot assay, cells were cultured with fresh medium for continued 24 h incubation. For cell viability measurement, cells were incubated with different amounts of CuB treatment for 72 h. The recombinant adenovirus containing GRP78 short hairpin RNA (shRNA) or negative control shRNAs (sh-NC) was packaged using pAdV-mCMV-miRNA-EGFP-SV40pA vector. The shRNAs for GRP78 were 5'-CTATTGCTGGCCTAAATGTTA-3' (shRNA-1), 5'-GTGTCATGGAACACTTCATCA-3' (shRNA-2), and

5'-TCCAAAGATTCAGCAACTGGT-3' (shRNA-3). The shRNA for negative control was 5'-AAATGTACTGCGCGTGGAGAC-3' (sh-NC). GRP78 over-expression was packaged with pAdV-mCMV-MCS-EGFP-SV40pA vector. GRP78 primer: Forward: 5'-CCGTAGAACGCAGATCGAATTCATGAACTCTCCCTGGTGGC-3', Reverse: 5'-TCCTCGCCCTTGCTCACCATGGCCAAC TCATCTTTTCTGCTGTATCC-3'.

2.15. Mouse tumor xenograft studies

Animal experiments were carried out according to the National Institutes of Health guidelines and the Association for Research in Vision and Ophthalmology guidelines. NCG mouse tumor xenograft experiments were conducted with the approval of the Institutional Animal Care and Use Committee (IACUC) of GemPharmatech Co., Ltd. (Nanjing, China) (Animal Protocol No. GPTAP20211021-7). After pre-experiment for several months, we finally selected CRMM2 cells (1 \times 10⁷ in 100 μ L of PBS with 20% Matrigel) to inject subcutaneously into male NCG mice (6–7 weeks old). Even so, the tumors in formal experiment mice still had poor growth, when the tumors reached a volume of \sim 50 mm³, the mice were randomized into treatment and control groups (seven mice per group). Mice in treatment groups received MEK162 (10 mg/kg, intragastric) or CuB (1 mg/kg, intragastric) five times per week for five weeks. One mouse died in the midnight of Day 23 in the 1 mg/kg CuB treatment group, which might be due to weight loss (no mouse died in the pre-experiment in the 1 mg/kg CuB treatment group).

The tumor size and body weight were monitored every 2 or 3 times per week. Tumor volume was calculated as 0.5 \times length \times width². Then, the tumor xenografts were removed and photographed. The blood samples were collected from submandibular venous plexus in NCG mice after being anesthetized.

2.16. Statistical analysis

Statistical analysis was performed using GraphPad Prism 8.0. The results were considered to be statistically significant at $P < 0.05$. For each separate set of assays, at least three independent experiments were evaluated. The results are represented as mean \pm standard deviation (SD).

3. Results

3.1. Effects of CuB on conjunctival melanoma phenotypes

Although CuB has been shown to impair cancer progression in a wide spectrum of human malignant cells, whether it is potent in suppressing conjunctival melanoma is unknown. We attempted to elucidate the role of CuB in different kinds of CM cells, including three CM cell lines obtained from Caucasian patients with a typical *NRAS* (CRMM2) or *BRAF* mutation (CRMM1 and CM2005.1) and one CM cell line obtained from a Han Chinese patient with typical *NRAS* mutation (CM-AS16)³⁷. Firstly, we determined the effect of CuB on the proliferation of conjunctival melanoma cells. Cell Counting Kit-8 (CCK-8) assay demonstrated that CuB impaired cell proliferation in CRMM2, CM-AS16, CRMM1 and CM2005.1 cells, with IC₅₀ values of 0.15, 0.08, 0.24 and 0.38 μ mol/L, respectively, without toxicity to the normal cells HL7702 (IC₅₀ > 100 μ mol/L, Table 1). MEK162, an orally available MEK inhibitor for the treatment of advanced cutaneous melanoma with *NRAS* mutation⁴¹, was chosen as the positive

control. Conjunctival melanoma cells are generally featured with poor growth both *in vitro* and *in vivo*, thus we explored the potential anti-cancer effect of CuB mainly on one cell line (CRMM2), additional cell lines will be introduced when it is absolutely necessary. Results also showed that the common cucurbitacins derivatives of CuB, including cucurbitacins D, E and I could inhibit CRMM2 cells proliferation at a comparable level (with IC_{50} doses ranging from 0.02 to 0.3 $\mu\text{mol/L}$, Supporting Information Fig. S1). Other derivatives *viz.* isocucurbitacin B, 23,24-dihydroisocucurbitacin B, cucurbitacins IIA and IIB did not show anti-proliferative potential against the CRMM2 cells ($IC_{50} > 50 \mu\text{mol/L}$, Fig. S1). It was inferred that the α - β -unsaturated ketone moiety in cucurbitacins structure rendered it functionality. Next, we analyzed the cell cycle transit and cell apoptosis post CuB treatment using flow cytometry. CRMM2 cells were treated with different doses of CuB for 24 h. It was observed that 0.1 and 0.2 $\mu\text{mol/L}$ CuB treatment induced a significant cell cycle arrest at G2/M phase, with inhibition of 24.0% and 37.5%, respectively (Fig. 1A). Meanwhile, CuB caused cell apoptosis in a dose-dependent manner, with apoptotic rate of 13.7% and 20.7%, respectively (Fig. 1B). Further, Western blot analysis was conducted to examine the protein expression level of cell cycle related proteins, especially those associated with G2/M phase. It was found that CuB significantly decreased the Cyclin B1 and CDK1 in these four CM cell lines, without changes in HL7702 cells (Fig. 1C). CuB also promoted an increase in the protein level of p21, independent of p53 activation (Supporting Information

Fig. S2). For apoptotic proteins analysis, CuB increased the expression of cleaved-PARP1 and decreased caspase-3, while other proteins including Bax and Bcl-2 were not changed too much at these concentrations in CRMM2 cells (Supporting Information Fig. S3). Taken together, we speculated that CuB (0.1 and 0.2 $\mu\text{mol/L}$) for 24 h mainly induced G2/M cell cycle arrest and Cyclin B1–CDK1 decreases in CM cells.

3.2. CuB decreased *KIF20A* via *FOXM1/PLK1* suppression

The anticancer mechanisms of CuB in different cancer cells have been widely investigated, yet the transcriptome profile exploring the mechanism of action of CuB is not entirely clear. Previous studies have identified several pathways that are influenced by CuB, including STAT3³¹, Hippo-YAP³³, Notch⁴² and ferroptosis⁴³. A genome-wide analysis of the genes that are significantly affected by CuB has not been reported till date. Besides, as mentioned above, more biomarkers and genetic information of conjunctival melanoma are still needed to be revealed. Hence, we conducted an RNA-seq analysis in CuB-treated CRMM2 cells at the concentrations of 0, 0.1 and 0.2 $\mu\text{mol/L}$. Venn diagram collectively indicated 32 genes as common differentially expressed genes (DEGs) between the two concentrations gradient CuB-treated groups ($P < 0.05$, Fig. 2A). Heatmap of these 32 genes revealed *KIF20A* transcriptional expression was most significantly decreased in a dose-dependent manner (fold change < 0.4 , adjusted $P < 10^{-5}$; Fig. 2B, and Supporting Information Table S1). The RNA-seq analysis quantifying

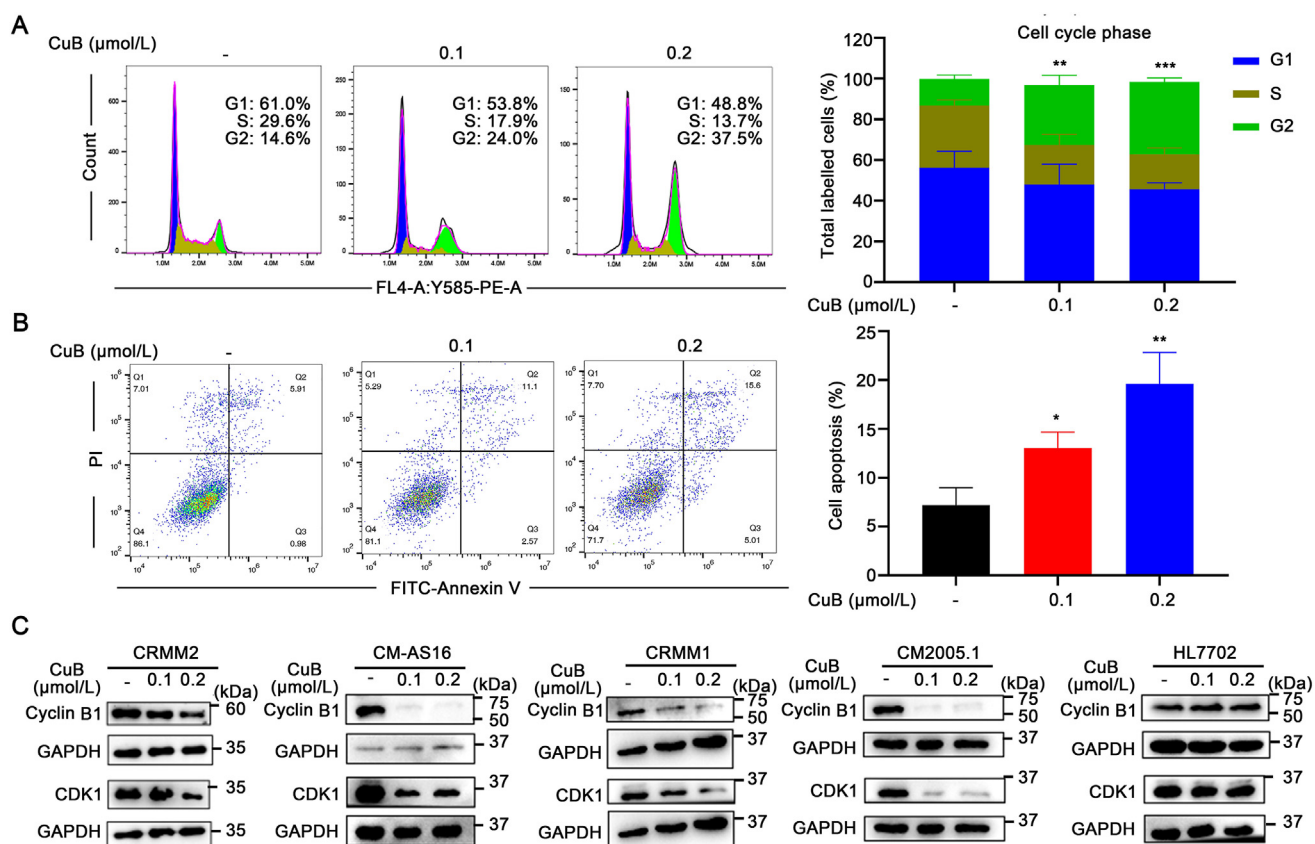


Figure 1 CuB impaired CM cells proliferation and caused G2/M cell cycle arrest. (A) and (B) represent flow cytometry analysis after treatment of CRMM2 cells with DMSO vehicle or CuB (0.1 and 0.2 $\mu\text{mol/L}$) for 24 h. Data are shown as mean \pm SD ($n = 3$) and compared using two-way ANOVA. * $P < 0.05$, ** $P < 0.01$, *** $P < 0.001$. (A) Cell cycle analysis. (B) Cell apoptosis measurement. (C) Immunoblotting of proteins involved in cell cycle in CM cells and HL7702 cells ($n = 3$). Data are representative of at least three independent experiments.

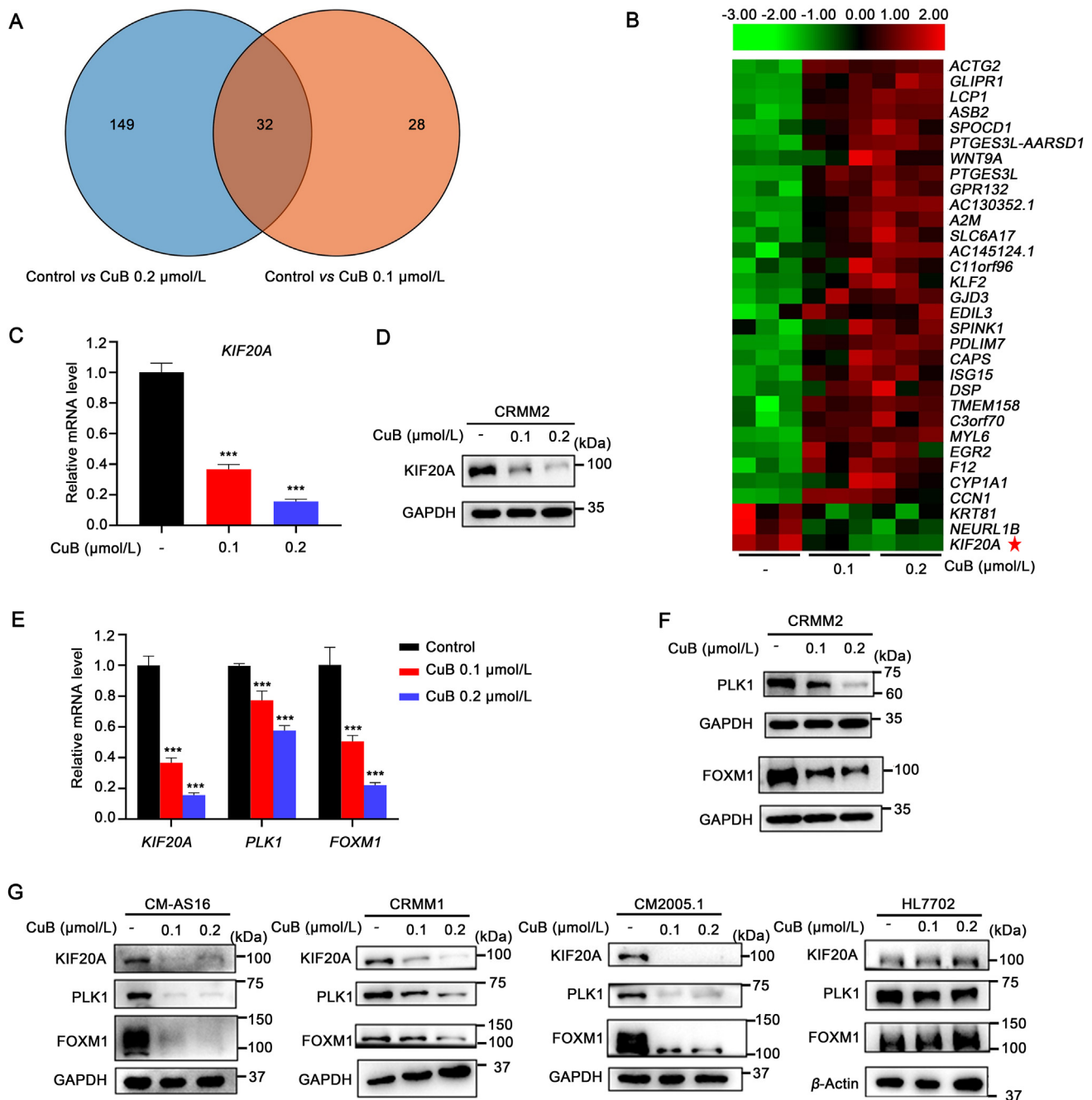


Figure 2 The effects of CuB on FOXM1/PLK1–KIF20A pathway in conjunctival melanoma cells were determined by transcriptomics, qRT-PCR and Western blot analysis. (A) Venn diagram showing the number of differentially expressed genes (DEGs) in each set of experiments, highlighting a total of 32 DEGs commonly identified from the two CuB-treated (0.1 and 0.2 $\mu\text{mol/L}$) sets of experiments ($n = 3$). (B) RNA sequencing cluster analysis chart of above 32 DEGs ($n = 3$). (C) and (D) KIF20A expression after CuB treatment (0.1 and 0.2 $\mu\text{mol/L}$). (C) Relative mRNA expression of *KIF20A* ($n = 3$), data represent three independent experiments. $***P < 0.001$, two-way ANOVA. (D) Protein expression of KIF20A ($n = 3$), data are representative of at least three independent experiments. (E) and (F) FOXM1 and PLK1 levels after CuB treatment (0.1 and 0.2 $\mu\text{mol/L}$). (E) Relative mRNA expression of *FOXM1* and *PLK1* ($n = 3$), data represent three independent experiments. $***P < 0.001$, two-way ANOVA. (F) Protein expression of FOXM1 and PLK1 ($n = 3$), data is representative of at least three independent experiments. (G) Protein expression of KIF20A, PLK1 and FOXM1 in CM-AS16, CRMM1, CM2005.1 and HL7702 cells ($n = 3$), data are representative of at least three independent experiments.

all genes expression demonstrated that *KIF20A* has a relative high expression in CRMM2 cells compared to genes such as *KRT81* and *NEURL1B*, thus *KIF20A* was selected for further observation. In fact, further experimental quantitative RT-PCR and Western blot

analysis indeed monitored KIF20A decreases after CuB treatment in CRMM2 cells (Fig. 2C and D).

KIF20A, also known as MKLP2 and RAB6KIFL, belongs to kinesin family and plays important roles in cell cycle and mitotic.

For cell cycle progression, PLK1 makes it indispensable, mainly through mitosis *via* its effects on chromosome segregation, spindle assembly, and cytokinesis⁴⁴. Evidences have disclosed that KIF20A is phosphorylated by PLK1 and in turn restricts the PLK1 localization to the central spindle during anaphase and telophase⁴⁵. KIF20A is also a potential downstream target of FOXM1, its expression was downregulated in the microarray analysis of FOXM1 siRNA⁴⁶. FOXM1 involves in mitotic progression and spindle formation by transcriptional regulation of a cluster of G2/M target genes. It is worth noting that the FOXM1 phosphorylation and activation depends on the PLK1–FOXM1 complex, which subsequently regulates its target genes including PLK1 itself⁴⁷. Thus, PLK1 and FOXM1 are essential effectors for KIF20A exerting its biological functions. Moreover, KIF20A, FOXM1 and PLK1 remain high expression in various types of tumors, and play multifunctional roles in cancer progression, thus representing attractive targets for cancer therapy^{44,48,49}. For our current study, it is tempting to speculate whether CuB treatment could influence the expression of PLK1 and FOXM1.

As shown in Table S1, the mRNA expression of *PLK1* and *FOXM1* were both decreased in RNA-seq analysis. Later qRT-PCR method revealed that the transcriptional expression of both *PLK1* and *FOXM1* genes significantly decreased upon CuB treatment, in a dose-dependent manner (Fig. 2E). Likewise, a significant dose-dependent decrease in PLK1 and FOXM1 at the protein level was also observed (Fig. 2F). To explore whether the anti-cancer effects of CuB in CRMM2 cells is applicable to other types of CM cells too, CM-AS16, CRMM1 and CM2005.1 were employed for CuB treatment. As shown in Fig. 2G, CuB treatment in these CM cells all blocked the protein expression of FOXM1, PLK1 and KIF20A. However, CuB failed to inhibit FOXM1/PLK1–KIF20A pathway in normal cells HL7702 (Fig. 2G). These experimental evidences suggested that CuB decreased KIF20A *via* FOXM1/PLK1 suppression and then induced CM cells G2/M phase inhibition.

3.3. ABPP to map the CuB-target protein GRP78 in cells

The prominent restriction of CuB on FOXM1–KIF20A axis initiating G2/M cell cycle arrest in CM cells provided a stimulus for subsequent direct target identification. We employed a chemical proteomics strategy called ABPP to map the direct targets of CuB within a cellular context (Fig. 3A). ABPP requires active and inactive probes, each bearing a reaction group for covalent binding to the protein target and a reporter group or “click” handles for bioorthogonal tag ligation for protein enrichment by affinity chromatography. We were prompted that the α - β -unsaturated ketone moiety in CuB structure might function as a reaction group covalent binding to its target (Fig. S1). Besides, the inhibitory activity of cucurbitacins B, D, E and I suggested that both 25 α -OH and 25 α -OAc were tolerated in structure for anti-proliferation potential (Fig. S1). 2-OH or 16-OH position of CuB was selected to incorporate an “click” handle consistent of an alkyne group and five probes were finally synthesized (Supporting Information, Section chemical synthesis).

Various assays were employed to fully characterize the performance of these probes. First, we evaluated their anti-proliferation potential in CRMM2 cells. The results proved that **BP-2** inhibited CRMM2 cells growth with an IC₅₀ of 0.27 μ mol/L, which was comparable to CuB (IC₅₀ = 0.15 μ mol/L), but **BP-4** did not show potential anticancer activity towards CRMM2 cells (IC₅₀ > 50 μ mol/L). Hence, **BP-2** was used as the active probe,

BP-4 as the negative probe, other probes including **BP-1**, **-3** and **-5** were used as the medium probe (Fig. 3B). Next, we performed “click” reaction with different probes *in situ* to label the whole proteome. CRMM2 cells were treated with 0.2 μ mol/L of different probes for 3 h prior to the cell lysis. The cell lysates reacted with TAMRA-azide under CuAAC-mediated click reaction and were separated by SDS-PAGE. Following in-gel fluorescence scanning suggested that these probes can label different cellular targets (Fig. 3C). Compared to the negative probe **BP-4**, the active probe **BP-2** led to the more and stronger visible bands, while **BP-1**, **-3** and **-5** gave other sightseeing. This difference could be attributed to either the different modification sites or the different cellular activity. The labelling of proteins with **BP-2** was also shown to be dose-dependent in cell lysates (Fig. 3D), which suggested us to further excavate specified target proteins by pull down/silver staining experiments (Fig. 4A). Lastly, we performed cellular imaging to track the subcellular probe localizations of **BP-2** and **BP-4** in the live cells. Live CRMM2 cells were incubated with **BP-2** and **BP-4**, proceeded by cell fixation, permeabilization, and click-mediated ligation. **BP-2** and **BP-4** treated cell samples were directly imaged after washing extra fluorescent dye. The strong fluorescence signals were mainly observed outside the nucleus in **BP-2** treated sample, and dramatically decreased in the presence of parental compound CuB. **BP-4** treated sample gave slight fluorescence similar to the control ones with DMSO treatment (Fig. 3E). Hence, probe **BP-2** was capable of efficiently capturing the particular targets of CuB in CRMM2 cells.

To identify the potential cellular targets of **BP-2**, we employed a pull-down/LC–MS/MS-based target identification. Samples were conjugated with TAMRA–Biotin–N3, affinity enrichment with streptavidin miniprep columns and separated using SDS-PAGE. Silver staining showed that proteins at ~75 kDa position were enriched in **BP-2** treated group, but decreased in **BP-4** and CuB competitive groups (Fig. 4A). The band position of these proteins was consistent with those displaced in **BP-2** dose-dependent labeling experiments. This result demonstrated that the bands might be probe-targeted proteins instead of abundant non-specific labeling (Fig. 3D). LC–MS/MS analysis delivered a list of occupied binders, from which we filtered potential targets by combining differences in proteins identified in active probe samples but not or less in the two controls (intensity: negative = 0, **BP-2** > CuB). As seen in Table 2, among the nine proteins which met the criteria, 78 kDa glucose-regulated protein (GRP78) was reported to be upstream regulator of PLK1⁵⁰. In addition, GRP78 was located in the cytoplasm and endoplasmic reticulum (ER), which was in line with the imaging results (Fig. 3E). GRP78 has already been validated as a potential biomarker and therapeutic target in many types of cancers, suppressing cancer cells progression, proliferation, invasion, and metastasis⁵¹. Up-regulated GRP78 generally correlates with the increased cancer aggression and worsened patient prognosis⁵². GRP78 can translocate to the cytoplasm and cell membrane to form cell surface CS-GRP78 under the stress of unfolded proteins⁵³. Further pull down/WB analysis with the corresponding antibody identified GRP78 protein as the potential target (Fig. 4B). Thus, GRP78 was prioritized for more follow-up validation tasks.

3.4. Validation of CuB interaction with GRP78

Target validation was also done in different experiments. As seen in Fig. 5A, **BP-2** was demonstrated to successfully label with

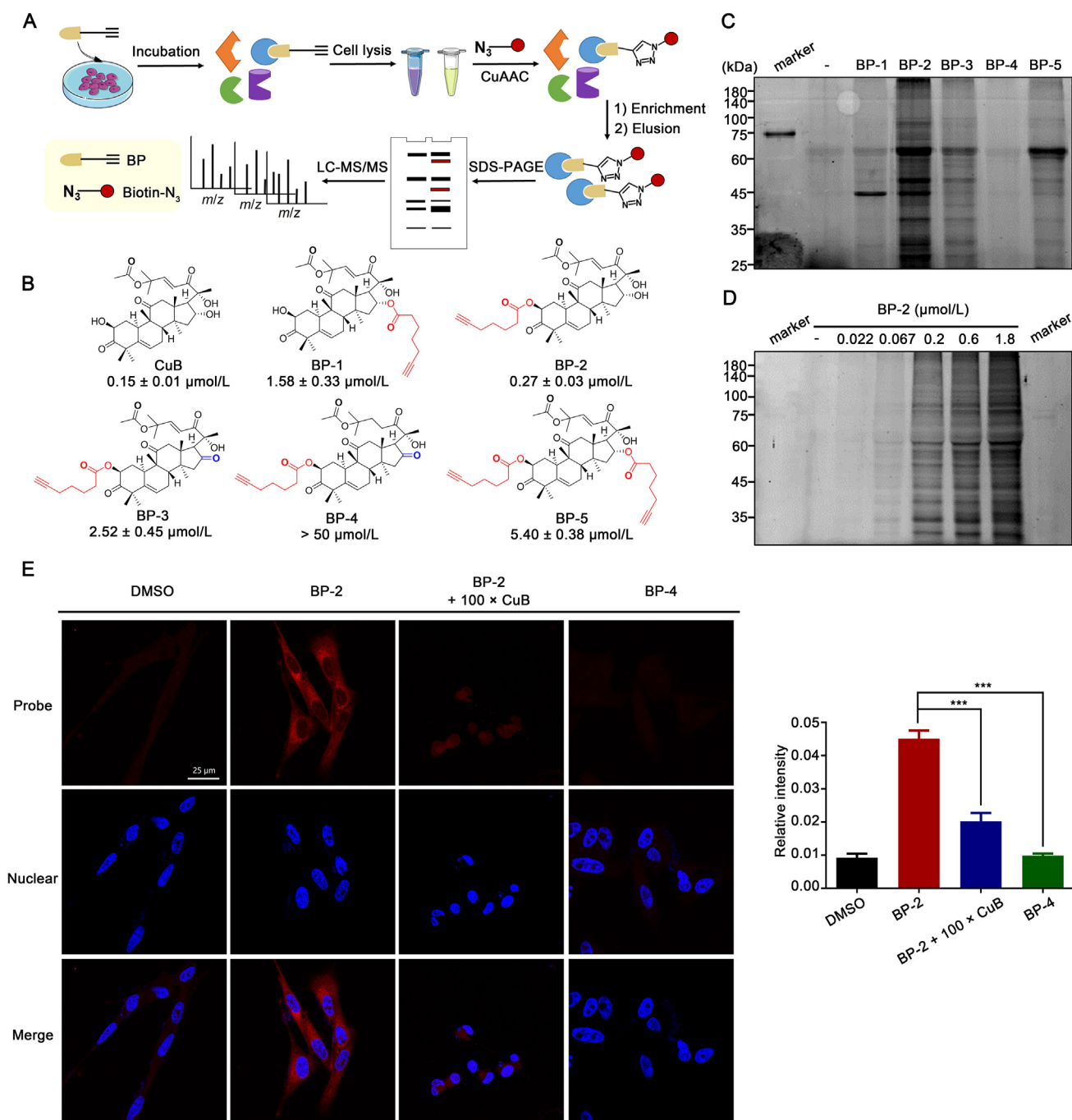


Figure 3 Biological activity of ABPP probes **BP-1–BP-5**. (A) Outline of the ABPP strategy for the target identification of small molecule probes in the live cells. After probes binding to their protein targets, a click reaction was performed to ligate a fluorophore or enrichment tag, such as biotin, to the probe. Enriched proteins were subsequently analyzed using Western blot or mass spectrometry. (B) Structures of ABPP probes **BP-1–BP-5** and their anti-proliferation potential towards CRMM2 cells based on CCK-8 assay ($n = 3$). (C) In gel fluorescence of active probe **BP-2**, inactive **BP-4** and medium probes **BP-1**, **BP-3** and **BP-5**, labelled CRMM2 proteome. Probe labelled proteins were ligated to TAMRA, separated by SDS-PAGE and visualized by in gel fluorescence ($n = 3$). (D) **BP-2** shows concentration-dependent labelling of protein targets. (E) Live cell imaging of CRMM2 cells with **BP-2/BP-4**, followed by cell fixation, permeabilization, click chemistry with TAMRA- N_3 , then image acquisition ($n = 10$). Blue: DAPI nuclear stain; red: TAMRA channel. Scale bar: 25 μm . All data are representative of at least three independent experiments.

recombinant GRP78 in a dose-dependent manner (left gel), and the fluorescence intensity of **BP-2** was relative with the amount of the identified protein (right gel), showing that probe **BP-2** possessed excellent sensitivity toward GRP78 protein. Thermal

shift binding assays proved that CuB treatment (0.2 $\mu\text{mol/L}$) increases the thermal stability of GRP78 in cell lysates in a temperature-dependent manner compared with DMSO and CuIIA controls (Fig. 5B). This indicated that there might be a direct

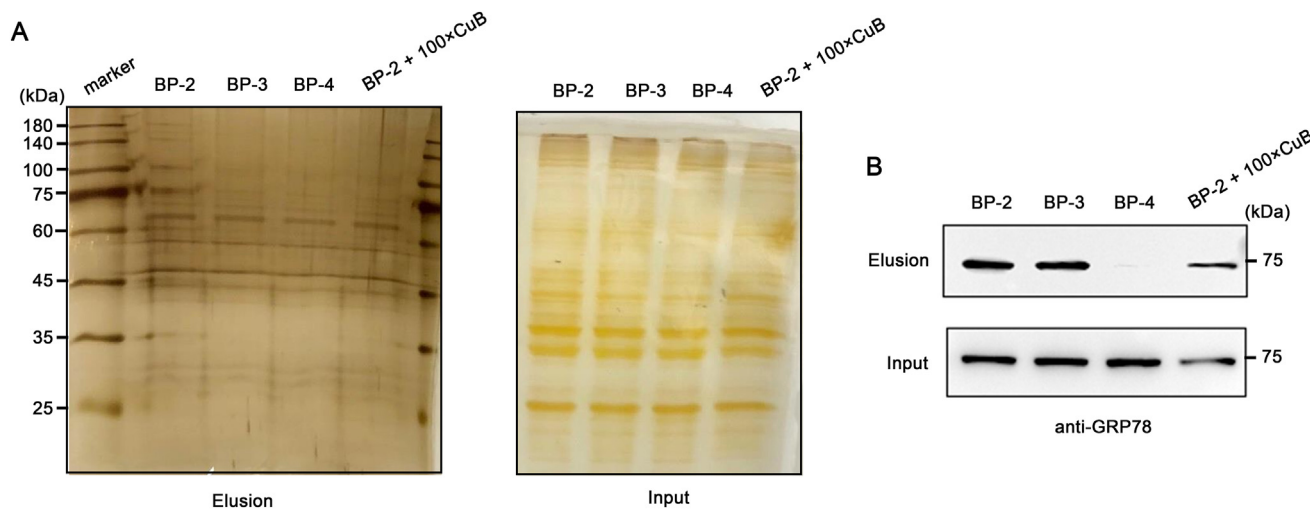


Figure 4 Target identification by probes **BP-2**, **BP-3** and **BP-4**. (A) Silver staining of probes **BP-2**, **BP-3** and **BP-4** (0.2 $\mu\text{mol/L}$) with or without competitor CuB (100 \times). Probe labelled proteins were labeled with biotin and enriched by streptavidin column, separated by SDS-PAGE and silver staining ($n = 3$). (B) Validation of the potential target GRP78 by pull-down/WB with probes **BP-2**, **BP-3** and **BP-4** (0.2 $\mu\text{mol/L}$) with or without competitor CuB (100 \times). All data are representative of at least three independent experiments.

interaction between GRP78 and CuB. Further microscale thermophoresis (MST) assays measured the ability of different concentrations of CuB to bind with GRP78, and revealed a potent K_d value of 0.11 $\mu\text{mol/L}$ (Fig. 5C), which was in line with the cellular activity. Our MS/MS analysis showed that a α - β -unsaturated ketone modification was present on the Lys326 site of GRP78 in the recombinant GRP78 samples with CuB treatment (Supporting Information Fig. S4). CuB showed weak binding affinity with mutant GRP78 (Lys326Ala), whose K_d value was 25.40 $\mu\text{mol/L}$ (Fig. 5C). Probe **BP-2** (1 and 5 $\mu\text{mol/L}$) can bind high amount of mutant GRP78 (5.40 $\mu\text{mol/L}$), indicating the weaker binding affinity between them (Supporting Information Fig. S5). Finally, we performed immunofluorescence (IF) experiments, displaying that **BP-2** (red) colocalized well with GRP78 (green) just outside the nucleus (Fig. 5D). These results further supported our previous speculation that CuB interacts with GRP78 and through the α - β -unsaturated ketone moiety.

GRP78 belongs to the HSP70-family proteins which requires ATP binding and hydrolysis to ensure their chaperone function. Thus, the ATPase enzymatic activity was evaluated both in the recombinant human GRP78 protein and cell lysates. CuB was found to inhibit the ATPase activity of GRP78 in recombinant human GRP78 protein and CRMM2 cells but invalid in HL7702 cells (Fig. 6A). The cell-free enzymatic activity inhibited by CuB was weaker than cell-based, might because the CRMM2

cellular microenvironment such as hypoxia, mutation and ER stress, can induce GRP78 overexpression and attract more CuB aggregation^{54,55}. To further assure whether CuB could influence the protein expression of GRP78 in CRMM2 cells, we conducted immunoblotting assays and confirmed that CuB did not perturb the protein level of GRP78 under the concentrations of 0.1 and 0.2 $\mu\text{mol/L}$ (Fig. 6B). Considering that neither CuB or **BP-2** bound with mutant GRP78 (Fig. 5C, and Fig. S5), we speculated that CuB directly binds to GRP78, disturbing its function and downstream pathway instead of decreasing its expression. In the following experiments, we evaluated how GRP78 knockdown or over-expression affected the biological processes of CM cells. CM cells have difficulties in common plasmid transfection, so we constructed series of recombinant adenovirus-packed shRNAs to infect CM cells. In fact, CuB treatment inhibited CRMM2 cells proliferation (sh-NC) at an IC_{50} value of 0.21 $\mu\text{mol/L}$, whereas GRP78 shRNA weakened this effect with IC_{50} values of 1.17 and 0.74 $\mu\text{mol/L}$, indicating the necessity of GRP78 for CuB anti-proliferation potential. It seems that GRP78 over-expression sensibitized CuB anti-tumor potential with an IC_{50} value of 0.14 $\mu\text{mol/L}$, compared to vector control (IC_{50} was 0.29 $\mu\text{mol/L}$). The sensibitization effect was not very remarkable might due to the high basal level of GRP78 itself in cells. Consistently, cell cycle analysis exhibited a disappeared G2/M phase suppression after CuB treatment with shRNAs, while GRP78 over-expression

Table 2 Protein hits identified by pull-down/LC-MS/MS with BP-2/BP-4/competitor CuB.

Protein name	Gene symbol	Location	Unique peptide
Histone H2B	HIST1H2BN	Nucleus	3
Histone H4	H4C1	Nucleus	5
Ig alpha-1 chain C region	IGHA1	Secreted	2
Dermcidin	DCD	Secreted	1
Ig gamma-2 chain C region	IGHG2	Secreted	1
Alpha-enolase	ENO1	Cytoplasm, membrane	3
78 kDa glucose-regulated protein	HSPA5/GRP78	Cytoplasm, ER	2
Interleukin-1 receptor antagonist protein	IL1RN	Cytoplasm, cytosol	1
Ubiquitin carboxyl-terminal hydrolase 31	USP31	Nucleus	1

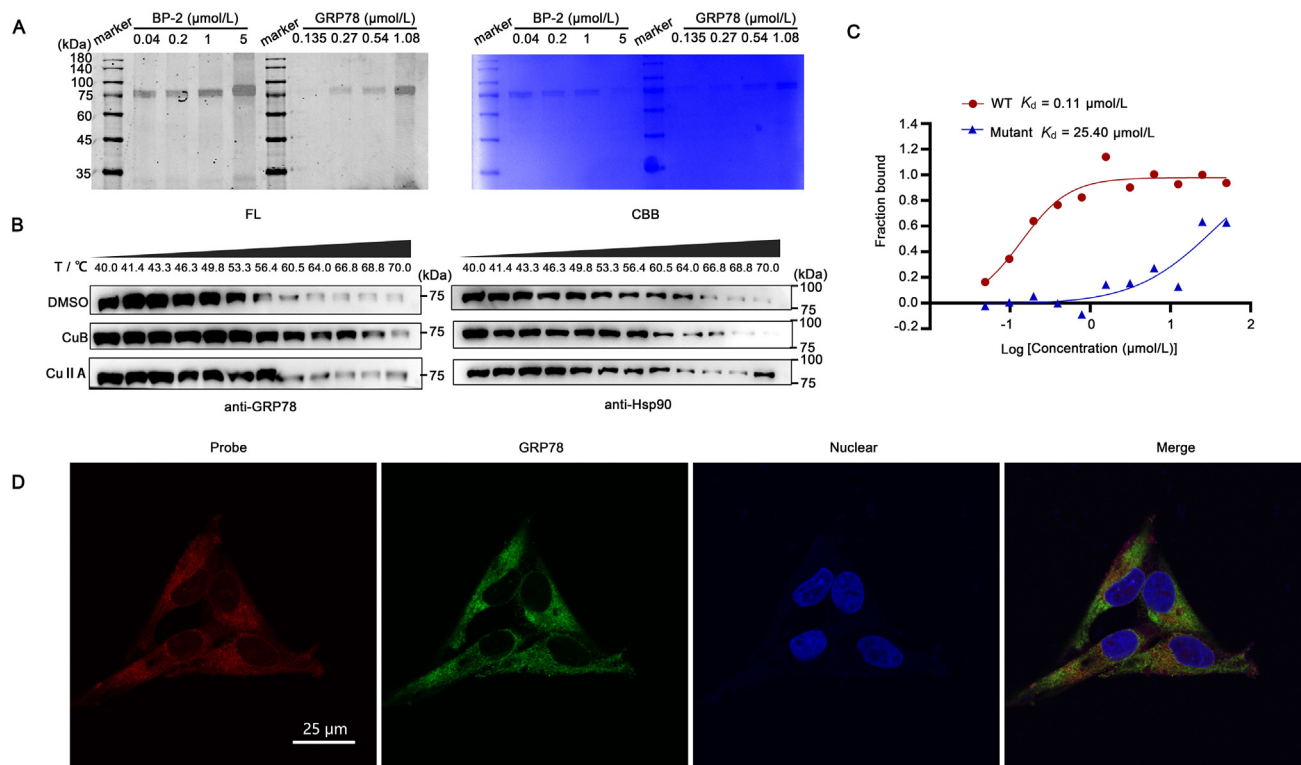


Figure 5 Target validation using different assays. (A) Labeling of recombinant GRP78 with BP-2 (different concentrations of BP-2 or different amounts of GRP78). Left: in gel fluorescence (FL). Right: Coomassie brilliant blue staining (CBB). (B) Cellular Thermal shift binding assay of CuB and CuIIA with GRP78-overexpressing 293 T cells ($n = 3$). (C) MST analysis of the binding affinity between CuB and human recombinant GRP78 protein (WT and mutant). The measured K_d value has been shown. (D) Imaging of CRMM2 cells with BP-2 and immunofluorescence against GRP78 ($n = 5$). Scale bar: 25 μm .

remains (Fig. 6C). In addition, GRP78 knockdown sharply reduced the expression of FOXM1, PLK1, KIF20A and Cyclin B1–CDK1 complex in conjunctival melanoma cells including CRMM2, CM-AS16, CRMM1 and CM2005.1 (Fig. 6D), suggesting CuB induced GRP78–FOXM1–KIF20A pathway blockage is applicable in CM cells with typical *NRAS* and *BRAF* mutation. Collectively, these data validated that the suppression effect of CuB on conjunctival melanoma cells G2/M phase mainly occurs through its binding and inhibition of GRP78 and that the decreased levels of GRP78 are deleterious to FOXM1–KIF20A pathway and cancer cells progression.

3.5. *In vivo* efficacy of CuB on CRMM2 xenograft tumors

Based on the *in vitro* findings described above, a conjunctival melanoma murine xenograft model was established to examine the *in vivo* anti-tumor effect of CuB in immunodeficient NCG mice. NCG mice come from knocking out the *Prkdc* and *Il2rg* genes in NOD/ShiJ mice through Crispr Cas9 technology. CRMM2 tumor-bearing mice were intragastric administrated with CuB (1 mg/kg), MEK162 (10 mg/kg) or control (vehicle) five times per week. At the end of the observation period, the mean tumor volume in the control group was 130 mm^3 compared to 94 mm^3 (1 mg/kg CuB), and 84 mm^3 (10 mg/kg MEK162). The tumor growth was significantly suppressed after treatment with CuB and MEK162, decreased by 16% and 33%, respectively, compared to the control group ($P < 0.001$) (Fig. 7A). To evaluate side effects, changes in the body weights in each group of mice were

monitored and recorded. As seen in Fig. 7B, CuB treatment did not affect the body weight of the mice obviously. Similarly, hemanalysis showed that there were no differences in the levels of alanine transaminase (ALT), aspartate transaminase (AST), creatinine (CREA) or urea (UREA) in mice serum of the drug-treated and control groups, indicating that CuB had no damage on liver and kidney functions (Table 3). Pathomorphological analysis of livers and kidneys in the treatment groups after a treatment period of five weeks was performed *via* H&E staining. No visible signs of toxicity or metastasis in internal organs were observed in all treated mice (Fig. 7C). Western blot analysis revealed that the expression levels of FOXM1, PLK1, and KIF20A were decreased in the CuB-treated group, accompanied by inhibition of G2/M cell cycle related proteins Cyclin B1 and CDK1 (Fig. 7D). Overall, our findings suggested that CuB exerts anti-tumor effects *in vivo* and should be further considered for conjunctival melanoma therapy.

4. Discussion

The development of the drugs for rare diseases (orphan drugs) has gradually become one of the major battlefields for the new drug research and development around the world. Many countries have introduced a combination of regulations and policies for the orphan drugs in the last two decades⁵⁶. In spite of these moves, still many rare diseases lack specific treatment regimens and patients are on the suffering end. Drug repurposing could be a potential alternative for the orphan drugs discovery, providing a

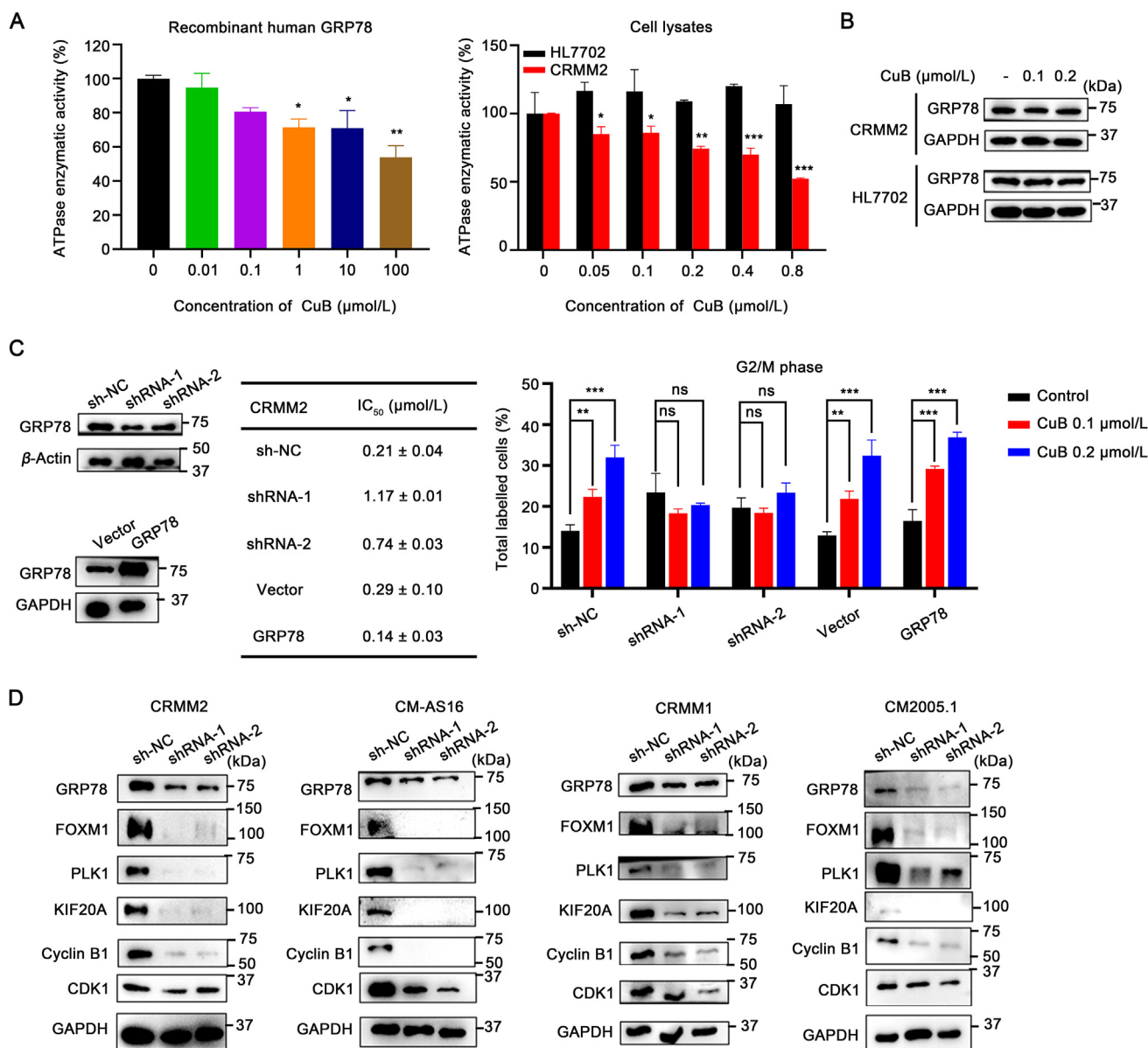


Figure 6 GRP78 as regulator of FOXM1–KIF20A pathway. (A) GRP78 activity measurement on recombinant GRP78 protein and cells lysates treated with different concentrations of CuB ($n = 3$). Left: Effects on purified recombinant GRP78 protein. Right: Effects on the CRMM2 and HL7702 cells lysates. The results are expressed as percentages of control (DMSO). (B) Immunoblotting for GRP78 in CRMM2 and HL7702 cells with or without CuB treatment ($n = 3$). (C) Effects of GRP78 knockdown or over-expression on CRMM2 cells proliferation and cell cycle. Left: Western blot of GRP78 after GRP78 shRNA and GRP78 over-expression infection. Middle: Effects on CRMM2 cells proliferation after CuB treatment with GRP78 shRNA and GRP78 over-expression infection (IC_{50} values). Right: Effects on G2/M cell cycle of CuB treatment (0.1 and 0.2 $\mu\text{mol/L}$) after GRP78 shRNA and GRP78 over-expression infection in CRMM2 cells. Data are mean \pm SD, $n = 3$; ns, no significance; $**P < 0.01$; $***P < 0.001$ compared to sh-NC control group, two-way ANOVA. (D) The expression of proteins *viz.* FOXM1, PLK1, KIF20A, CyclinB1 and CDK1 was decreased in CRMM2, CM-AS16, CRMM1 and CM2005.1 cells after treatment with shGRP78s ($n = 3$).

faster path for an approved drug to come to the market in a shorter span of time, less risky and less costly than the completely new drugs⁵⁷. Opportunities of drug repurposing have often been identified serendipitously through novel clinical observations, but it seems unreasonable for rare disease including CM. Thus, our group consciously screened our in-house collected marketed drugs with anti-CM potential using a cellular proliferation assay²⁷. To our excitement, some drugs indeed inhibited CM cells growth, from which we selected CuB, a traditional medicine of adjuvant therapy for liver cancer, for further investigation.

CuB has been proven for various pharmacological effects especially against tumors, which ensured us that it could also inhibit CM incontrovertibly. Initial phenotypic validation of CuB against CRMM2 cells growth inspired us to explore its in-depth mechanism. The mechanism, how the CuB modulates the whole transcriptional profile has not yet been established, as well as the upstream regulators. We, therefore, conducted an RNA-Seq assay and revealed KIF20A as the most down-regulated gene after CuB treatment. This dysregulation was found to be induced by the FOXM1 and PLK1 inhibition, leading to the entire axis effected

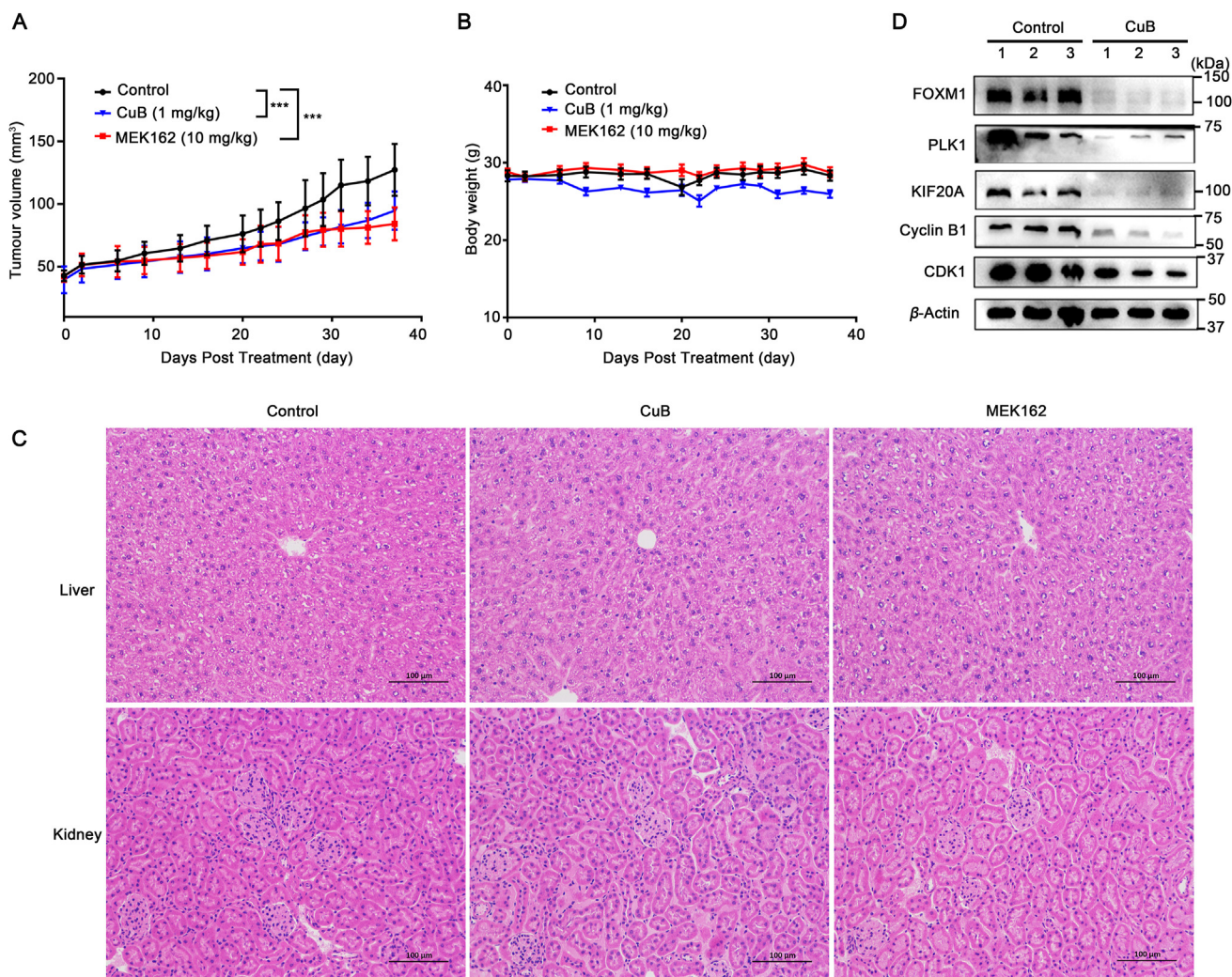


Figure 7 *In vivo* anti-tumor effect of CuB. Mice were intragastric administrated with CuB (1 mg/kg), MEK162 (10 mg/kg) or vehicle for 5 weeks ($n = 7$). One mouse died in the midnight of Day 23 under 1 mg/kg CuB treatment. After 5 weeks, all the mice were sacrificed and the tumors were excised for analysis. (A) Tumor volume of mice from each group. (B) Body weight of mice from each group during the whole observation period. (C) The representative images of H&E staining of liver and kidney from mice in each group at the end of the observation period. Scale bar: 100 μm . (D) Effects on protein expression of FOXM1–KIF20A pathway in CRMM2 tumor tissues. Data are presented as the mean \pm SD, *** $P < 0.001$ vs. the control group by two-way ANOVA using GraphPad Prism 8.0 ($n = 7$).

by CuB. KIF20A is upregulated in multiple cancers and plays important roles in promoting malignant behavior, however, it is for the first time, its role has been deciphered in CM. FOXM1 is a transcriptional factor, regulating the expression of cell cycle genes essential for DNA replication and mitosis, such as Cyclin B1 and

CDK1. FOXM1 also functions as a direct binding partner of PLK1, controlling a G2/M transcriptional programme⁴⁷.

Target identification demonstrated GRP78 as one of the potential targets of CuB, different from previous reports^{31,33,42,43}. GRP78 belongs to the heat shock protein 70 (HSP70) family, functions as endoplasmic reticulum chaperone involved in the folding and assembly of proteins⁵¹. It has been hypothesized GRP78 to be a therapeutic target for various forms of cancer. In this work, CuB was shown to bind with GRP78 and had a covalent modification of the α - β -unsaturated ketone moiety. This modification might somehow induce the conformational changes of GRP78 protein, which needs to be further investigation. GRP78 has a high binding affinity with ATP, its ATPase activity will be stimulated when binding to the unfolded protein, which in turn catalyzes proteins re-folding. We found that CuB was able to inhibit the ATPase activity of GRP78 in a dose-dependent manner, leading to the suppression of its downstream pathway. Our work further showed that knockdown of GRP78 could lead to the

Table 3 Blood level of different biochemical parameters among different groups.

Group	ALT (IU/L)	AST (IU/L)	UREA (mmol/L)	CREA ($\mu\text{mol/L}$)
Normal	21–76	42–169	3.8–13.1	10.6–23.0
Control	21.6 \pm 2.6	84.2 \pm 8.4	8.0 \pm 0.7	18.0 \pm 2.1
CuB	30.2 \pm 11.1	123.0 \pm 37.9	9.2 \pm 1.0	16.5 \pm 1.4
MEK162	32.9 \pm 30.7	106.5 \pm 44.0	101 \pm 1.7	15.1 \pm 1.7

Normal refers to the reference range of each index in mice of the same age. Data are shown as mean \pm SD; $n = 6$ for CuB treatment, $n = 7$ for control and MEK162 treatment.

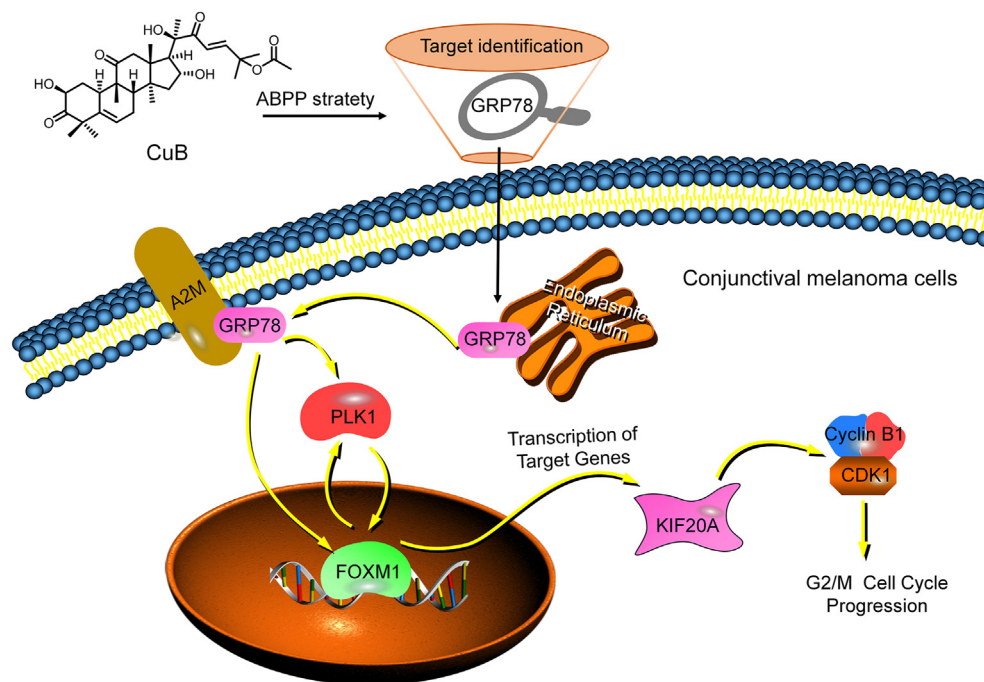


Figure 8 Schematic representation of mechanism by which CuB regulates the GRP78–FOXM1–KIF20A pathway.

modulation of the FOXM1–KIF20A pathway and its downstream G2/M cell cycle arrest. *In vivo* CRMM2 xenograft model showed that CuB suppressed tumors growth without obvious side effects. Keeping this in view, the identification of CuB as a novel GRP78–FOXM1–KIF20A disturber is an important finding which could further be explored and supported by expanding the toolbox available to interrogate GRP78 biology, as well as the CuB application into conjunctival melanoma and other tumors therapy.

5. Conclusions

Our findings in the present study indicated that traditional medicine CuB exerted potential anti-proliferation and G2/M cell cycle arrest effects in a rare ocular tumor named CM. Mechanistically, CuB suppressed conjunctival melanoma cells growth by targeting GRP78 protein and thereby downregulating the GRP78/FOXM1/KIF20A signaling pathway (Fig. 8). GRP78, FOXM1 and KIF20A have been reported to be overexpressed in various malignant tumors and unfriendly to oncotherapy. This work paved the way for the first connection of GRP78, FOXM1 and KIF20A in CuB stimulation as well as provided an alternative mechanism for further clinical exploration in CM. Excitingly, evidences we displayed in this research might facilitate a new approach to deliver a GRP78/FOXM1/KIF20A modulator to benefit all CM patients.

Acknowledgments

This work was supported by the National Mega-project for Innovative Drugs of China (2019ZX09721001-004-003), the National Natural Science Foundation of China (82003603 and 81872747), the Innovative Research Team of High-level Local Universities in Shanghai, the National Special Fund for State Key Laboratory of Bioreactor Engineering (2060204, China), Shanghai

Frontiers Science Center of Optogenetic Techniques for Cell Metabolism (2021 Sci & Tech 03-28, China).

Author contributions

Jian Li and Xiaofang Xu contributed to the design of the research, revised the manuscript and provided financial support. Jinlian Wei, Xin Chen and Yongyun Li performed the experiments and analyzed the data. Ruoxi Li, Keting Bao, Liang Liao, Yuqing Xie and Tiannuo Yang helped to perform the experiments. Jin Zhu, Fei Mao, Shuaishuai Ni and Renbing Jia helped to revised it critically for important intellectual content. All the authors have approved the final version of the manuscript.

Conflicts of interest

The authors declare no conflicts of interest.

Appendix A. Supporting information

Supporting data to this article can be found online at <https://doi.org/10.1016/j.apsb.2022.05.021>.

References

1. McCartney AC. Pathology of ocular melanomas. *Br Med Bull* 1995; **51**:678–93.
2. Scotto J, Fraumeni JF Jr, Lee JA. Melanomas of the eye and other noncutaneous sites: epidemiologic aspects. *J Natl Cancer Inst* 1976; **56**:489–91.
3. Vora GK, Demirci H, Marr B, Mruthyunjaya P. Advances in the management of conjunctival melanoma. *Surv Ophthalmol* 2017; **62**:26–42.
4. Finger PT, Sedeek RW, Chin KJ. Topical interferon alfa in the treatment of conjunctival melanoma and primary acquired melanosis complex. *Am J Ophthalmol* 2008; **145**:124–9.

5. Ditta LC, Shildkrot Y, Wilson MW. Outcomes in 15 patients with conjunctival melanoma treated with adjuvant topical mitomycin C: complications and recurrences. *Ophthalmology* 2011;**118**:1754–9.
6. Grimes JM, Shah NV, Samie FH, Carvajal RD, Marr BP. Conjunctival melanoma: current treatments and future options. *Am J Clin Dermatol* 2020;**21**:371–81.
7. Pearson G, Robinson F, Beers Gibson T, Xu BE, Karandikar M, Berman K, et al. Mitogen-activated protein (MAP) kinase pathways: regulation and physiological functions. *Endocr Rev* 2001;**22**:153–83.
8. Munoz-Couselo E, Adelantado EZ, Ortiz C, Garcia JS, Perez-Garcia J. *NRAS*-mutant melanoma: current challenges and future prospect. *OncoTargets Ther* 2017;**10**:3941–7.
9. Spendlove HE, Damato BE, Humphreys J, Barker KT, Hiscott PS, Houlston RS. *BRAF* mutations are detectable in conjunctival but not uveal melanomas. *Melanoma Res* 2004;**14**:449–52.
10. Lake SL, Jmor F, Dopierala J, Taktak AF, Coupland SE, Damato BE. Multiplex ligation-dependent probe amplification of conjunctival melanoma reveals common *BRAF* V600E gene mutation and gene copy number changes. *Invest Ophthalmol Vis Sci* 2011;**52**:5598–604.
11. Goldenberg-Cohen N, Cohen Y, Rosenbaum E, Herscovici Z, Chowers I, Weinberger D, et al. T1799A *BRAF* mutations in conjunctival melanocytic lesions. *Invest Ophthalmol Vis Sci* 2005;**46**:3027–30.
12. Gear H, Williams H, Kemp EG, Roberts F. *BRAF* mutations in conjunctival melanoma. *Invest Ophthalmol Vis Sci* 2004;**45**:2484–8.
13. Scholz SL, Cosgarea I, Susskind D, Murali R, Moller I, Reis H, et al. *NF1* mutations in conjunctival melanoma. *Br J Cancer* 2018;**118**:1243–7.
14. Griewank KG, Westkemper H, Murali R, Mach M, Schilling B, Wiesner T, et al. Conjunctival melanomas harbor *BRAF* and *NRAS* mutations and copy number changes similar to cutaneous and mucosal melanomas. *Clin Cancer Res* 2013;**19**:3143–52.
15. Rossi E, Schinzari G, Maiorano BA, Pagliara MM, Di Stefani A, Bria E, et al. Conjunctival melanoma: genetic and epigenetic insights of a distinct type of melanoma. *Int J Mol Sci* 2019;**20**:5447–63.
16. Cao J, Heijkants RC, Jochemsen AG, Dogrusoz M, de Lange MJ, van der Velden PA, et al. Targeting of the MAPK and AKT pathways in conjunctival melanoma shows potential synergy. *Oncotarget* 2017;**8**:58021–36.
17. Maleka A, Astrom G, Bystrom P, Ullenhag GJ. A case report of a patient with metastatic ocular melanoma who experienced a response to treatment with the *BRAF* inhibitor vemurafenib. *BMC Cancer* 2016;**16**:634.
18. Rossi E, Maiorano BA, Pagliara MM, Sammarco MG, Dosa T, Martini M, et al. Dabrafenib and trametinib in *BRAF* mutant metastatic conjunctival melanoma. *Front Oncol* 2019;**9**:232.
19. Pinto Torres S, Andre T, Gouveia E, Costa L, Passos MJ. Systemic treatment of metastatic conjunctival melanoma. *Case Rep Oncol Med* 2017;**2017**:4623964.
20. Haendel M, Vasilevsky N, Unni D, Bologna C, Harris N, Rehm H, et al. How many rare diseases are there?. *Nat Rev Drug Discov* 2020;**19**:77–8.
21. Sun W, Xie Z, Liu Y, Zhao D, Wu Z, Zhang D, et al. JX06 selectively inhibits pyruvate dehydrogenase kinase PDK1 by a covalent cysteine modification. *Cancer Res* 2015;**75**:4923–36.
22. Huang Z, Li R, Tang T, Ling D, Wang M, Xu D, et al. A novel multistage antiparasitodal inhibitor targeting *Plasmodium falciparum* histone deacetylase 1. *Cell Discov* 2020;**6**:93.
23. Li R, Ling D, Tang T, Huang Z, Wang M, Ding Y, et al. Discovery of novel *Plasmodium falciparum* HDAC1 inhibitors with dual-stage antimalarial potency and improved safety based on the clinical anticancer drug candidate quisinostat. *J Med Chem* 2021;**64**:2254–71.
24. Chen F, Di H, Wang Y, Cao Q, Xu B, Zhang X, et al. Small-molecule targeting of a diapophytoene desaturase inhibits *S. aureus* virulence. *Nat Chem Biol* 2016;**12**:174–9.
25. Li X, Lu J, Xu Y, Wang J, Qiu X, Fan L, et al. Discovery of nitazoxanide-based derivatives as autophagy activators for the treatment of Alzheimer's disease. *Acta Pharm Sin B* 2020;**10**:646–66.
26. Mao Z, Liu W, Huang Y, Sun T, Bao K, Feng J, et al. Anti-aging effects of chlorpropamide depend on mitochondrial complex-II and the production of mitochondrial reactive oxygen species. *Acta Pharm Sin B* 2022;**12**:665–77.
27. Bao K, Li Y, Wei J, Li R, Yang J, Shi J, et al. Fangchinoline suppresses conjunctival melanoma by directly binding FUBP2 and inhibiting the homologous recombination pathway. *Cell Death Dis* 2021;**12**:380.
28. Liang J, Chen D. Advances in research on the anticancer mechanism of the natural compound cucurbitacin from Cucurbitaceae plants: a review. *Tradit Chin Med* 2019;**4**:68–81.
29. Raikhlin-Eisenkraft B, Bentur Y. *Ecbalium elaterium* (squirting cucumber)—remedy or poison?. *J Toxicol Clin Toxicol* 2000;**38**:305–8.
30. Kim KH, Lee IS, Park JY, Kim Y, An EJ, Jang HJ. Cucurbitacin B induces hypoglycemic effect in diabetic mice by regulation of AMP-activated protein kinase alpha and glucagon-like peptide-1 via bitter taste receptor signaling. *Front Pharmacol* 2018;**9**:1071.
31. Chan KT, Li K, Liu SL, Chu KH, Toh M, Xie WD. Cucurbitacin B inhibits STAT3 and the Raf/MEK/ERK pathway in leukemia cell line K562. *Cancer Lett* 2010;**289**:46–52.
32. Xu J, Chen Y, Yang R, Zhou T, Ke W, Si Y, et al. Cucurbitacin B inhibits gastric cancer progression by suppressing STAT3 activity. *Arch Biochem Biophys* 2020;**684**:108314.
33. Chai Y, Xiang K, Wu Y, Zhang T, Liu Y, Liu X, et al. Cucurbitacin B inhibits the Hippo–YAP signaling pathway and exerts anticancer activity in colorectal cancer cells. *Med Sci Mon Int Med J Exp Clin Res* 2018;**24**:9251–8.
34. Kaewmeesri P, Kukongviriyapan V, Prawan A, Kongpetch S, Senggunprai L. Cucurbitacin B diminishes metastatic behavior of cholangiocarcinoma cells by suppressing focal adhesion kinase. *Asian Pac J Cancer Prev APJCP* 2021;**22**:219–25.
35. Qu Y, Cong P, Lin C, Deng Y, Li-Ling J, Zhang M. Inhibition of paclitaxel resistance and apoptosis induction by cucurbitacin B in ovarian carcinoma cells. *Oncol Lett* 2017;**14**:145–52.
36. Kausar H, Munagala R, Bansal SS, Aqil F, Vadhanam MV, Gupta RC. Cucurbitacin B potently suppresses non-small-cell lung cancer growth: identification of intracellular thiols as critical targets. *Cancer Lett* 2013;**332**:35–45.
37. Li Y, Shang Q, Li P, Cao J, Zhu L, Jager MJ, et al. Characterization of a conjunctival melanoma cell line CM-AS16, newly-established from a metastatic Han Chinese patient. *Exp Eye Res* 2018;**173**:51–63.
38. Jazayeri SM, Melgarejo Muñoz LM, Romero HM. RNA-Seq: a glance at technologies and methodologies. *Acta Biol Colomb* 2015;**20**:23–35.
39. Wilkinson IVL, Perkins KJ, Dugdale H, Moir L, Vuorinen A, Chatzopoulou M, et al. Chemical proteomics and phenotypic profiling identifies the aryl hydrocarbon receptor as a molecular target of the Utrrophin Modulator Ezutromid. *Angew Chem Int Ed Engl* 2020;**59**:2420–8.
40. Cerezo M, Lehraiki A, Millet A, Rouaud F, Plaisant M, Jaune E, et al. Compounds triggering ER stress exert anti-melanoma effects and overcome *BRAF* inhibitor resistance. *Cancer Cell* 2016;**29**:805–19.
41. Queirolo P, Spagnolo F. Binimetinib for the treatment of *NRAS*-mutant melanoma. *Expert Rev Anticancer Ther* 2017;**17**:985–90.
42. Dandawate P, Subramaniam D, Panovich P, Standing D, Krishnamachary B, Kaushik G, et al. Cucurbitacin B and I inhibits colon cancer growth by targeting the Notch signaling pathway. *Sci Rep* 2020;**10**:1290.
43. Huang S, Cao B, Zhang J, Feng Y, Wang L, Chen X, et al. Induction of ferroptosis in human nasopharyngeal cancer cells by cucurbitacin B: molecular mechanism and therapeutic potential. *Cell Death Dis* 2021;**12**:237.
44. de Carcer G, Manning G, Malumbres M. From Plk1 to Plk5: functional evolution of polo-like kinases. *Cell Cycle* 2011;**10**:2255–62.
45. Neef R, Preisinger C, Sutcliffe J, Kopajtich R, Nigg EA, Mayer TU, et al. Phosphorylation of mitotic kinesin-like protein 2 by polo-like kinase 1 is required for cytokinesis. *J Cell Biol* 2003;**162**:863–75.
46. Wonsey DR, Follettie MT. Loss of the forkhead transcription factor FoxM1 causes centrosome amplification and mitotic catastrophe. *Cancer Res* 2005;**65**:5181–9.

47. Fu Z, Malureanu L, Huang J, Wang W, Li H, van Deursen JM, et al. Plk1-dependent phosphorylation of FoxM1 regulates a transcriptional programme required for mitotic progression. *Nat Cell Biol* 2008;**10**:1076–82.
48. Wu WD, Yu KW, Zhong N, Xiao Y, She ZY. Roles and mechanisms of Kinesin-6 KIF20A in spindle organization during cell division. *Eur J Cell Biol* 2019;**98**:74–80.
49. Halasi M, Gartel AL. Targeting FOXM1 in cancer. *Biochem Pharmacol* 2013;**85**:644–52.
50. Gopal U, Gonzalez-Gronow M, Pizzo SV. Activated alpha2-macroglobulin regulates transcriptional activation of c-MYC target genes through cell surface GRP78 protein. *J Biol Chem* 2016;**291**:10904–15.
51. Bailly C, Waring MJ. Pharmacological effectors of GRP78 chaperone in cancers. *Biochem Pharmacol* 2019;**163**:269–78.
52. Nagelkerke A, Bussink J, Sweep FC, Span PN. The unfolded protein response as a target for cancer therapy. *Biochim Biophys Acta* 2014;**1846**:277–84.
53. Elfiky AA, Baghdady AM, Ali SA, Ahmed MI. GRP78 targeting: hitting two birds with a stone. *Life Sci* 2020;**260**:118317.
54. Ninkovic S, Harrison SJ, Quach H. Glucose-regulated protein 78 (GRP78) as a potential novel biomarker and therapeutic target in multiple myeloma. *Expert Rev Hematol* 2020;**13**:1201–10.
55. Kharabi Masouleh B, Geng H, Hurtz C, Chan LN, Logan AC, Chang MS, et al. Mechanistic rationale for targeting the unfolded protein response in pre-B acute lymphoblastic leukemia. *Proc Natl Acad Sci U S A* 2014;**111**:E2219–28.
56. Mariz S, Reese JH, Westermark K, Greene L, Goto T, Hoshino T, et al. Worldwide collaboration for orphan drug designation. *Nat Rev Drug Discov* 2016;**15**:440–1.
57. Tambuyzer E, Vandendriessche B, Austin CP, Brooks PJ, Larsson K, Miller Needleman KI, et al. Therapies for rare diseases: therapeutic modalities, progress and challenges ahead. *Nat Rev Drug Discov* 2020;**19**:93–111.